

# Isotropic Cooper Pairs with Emergent Sign Changes in Single-Layer Iron Superconductor

J.P. Rodriguez<sup>1</sup>

<sup>1</sup>*Department of Physics and Astronomy,  
California State University, Los Angeles, California 90032*

## Abstract

We model a single layer of heavily electron-doped FeSe by spin-1/2 moments over a square lattice of iron atoms that include the  $3d_{xz}$  and  $3d_{yz}$  orbitals, at strong on-site Coulomb repulsion. Above half filling, we find emergent hole bands below the Fermi level at the center of the one-iron Brillouin zone in a half metal state characterized by hidden magnetic order and by electron-type Fermi surface pockets at wavenumbers that double the unit cell along the principal axes. “Replicas” of the emergent hole bands exist at lower energy in the two-iron Brillouin zone. Exact calculations with two mobile electrons find evidence for isotropic Cooper pairs that alternate in sign between the electron bands and the emergent hole bands.

*Introduction.* The discovery of superconductivity in iron-pnictide materials has uncovered a new path in the search for high-temperature superconductors[1]. Superconductivity has been observed recently in a single layer of FeSe on a doped SrTiO<sub>3</sub> (STO) substrate[2–4] below critical temperatures as high as 100 K [5]. Electronic conduction originates from the 3d orbitals of the iron atoms, which form a square lattice. Angle-resolved photo-emission spectroscopy(ARPES), in particular, reveals circular electron-type Fermi surface pockets centered at wave numbers  $(\pi/a)\hat{x}$  and  $(\pi/a)\hat{y}$  that lie along the principal axes of the iron lattice, where  $a$  is the lattice constant[6, 7]. Unlike the case of most iron-pnictide materials, however, ARPES also finds that hole bands centered at zero two-dimensional (2D) momentum lie well below the Fermi level in the case of single-layer FeSe/STO. At low temperature, it also finds an isotropic gap at the electron Fermi surface pockets[8, 9], which is confirmed by scanning tunneling microscopy (STM)[10]. The same set of phenomena have been recently observed below critical temperatures in the range 40-50 K at the surfaces of intercalated FeSe[11–13], of alkali-metal doped FeSe[14–17], and of voltage-gate tuned thin films of FeSe[18, 19]. Comparison with bulk FeSe, which has a much lower critical temperature of 8 K, strongly suggests that the high-temperature superconductivity exhibited above is due to a new 2D groundstate that appears after heavy electron doping.

Calculations based on the independent-electron approximation[20] fail to describe the Fermi surfaces in single-layer FeSe/STO. In particular, density-functional theory (DFT) typically predicts that the hole bands centered at zero 2D momentum cross the Fermi level[8, 11, 21]. DFT also fails to account for a nearby Mott insulator phase at low electron doping in voltage-gate tuned thin films of FeSe and in single-layer FeSe/STO[19, 22]. The previous suggests that the limit of strong electron-electron interactions[23, 24] is a better starting point to describe superconductivity in heavily electron-doped FeSe.

Below, we propose that the hole bands observed by ARPES below the Fermi level at the Brillouin zone center in a surface layer of FeSe are examples of emergent phenomena. The latter is revealed by both mean-field and exact calculations of the one-electron spectrum in a two-orbital  $t$ - $J$  model that includes only degenerate  $d_{xz}$  and  $d_{yz}$  electron bands centered at wavenumbers  $(\pi/a)\hat{y}$  and  $(\pi/a)\hat{x}$ , respectively, in the one-iron Brillouin zone. Local spin-1/2 moments live on  $d_{(x\pm iy)z}$  orbitals, on the other hand, which yields isotropic magnetism. Emergent hole bands approach the Fermi level at zero 2D momentum as Hund coupling increases inside of a half metal phase that is characterized by hidden Néel order per  $d_{(x\pm iy)z}$

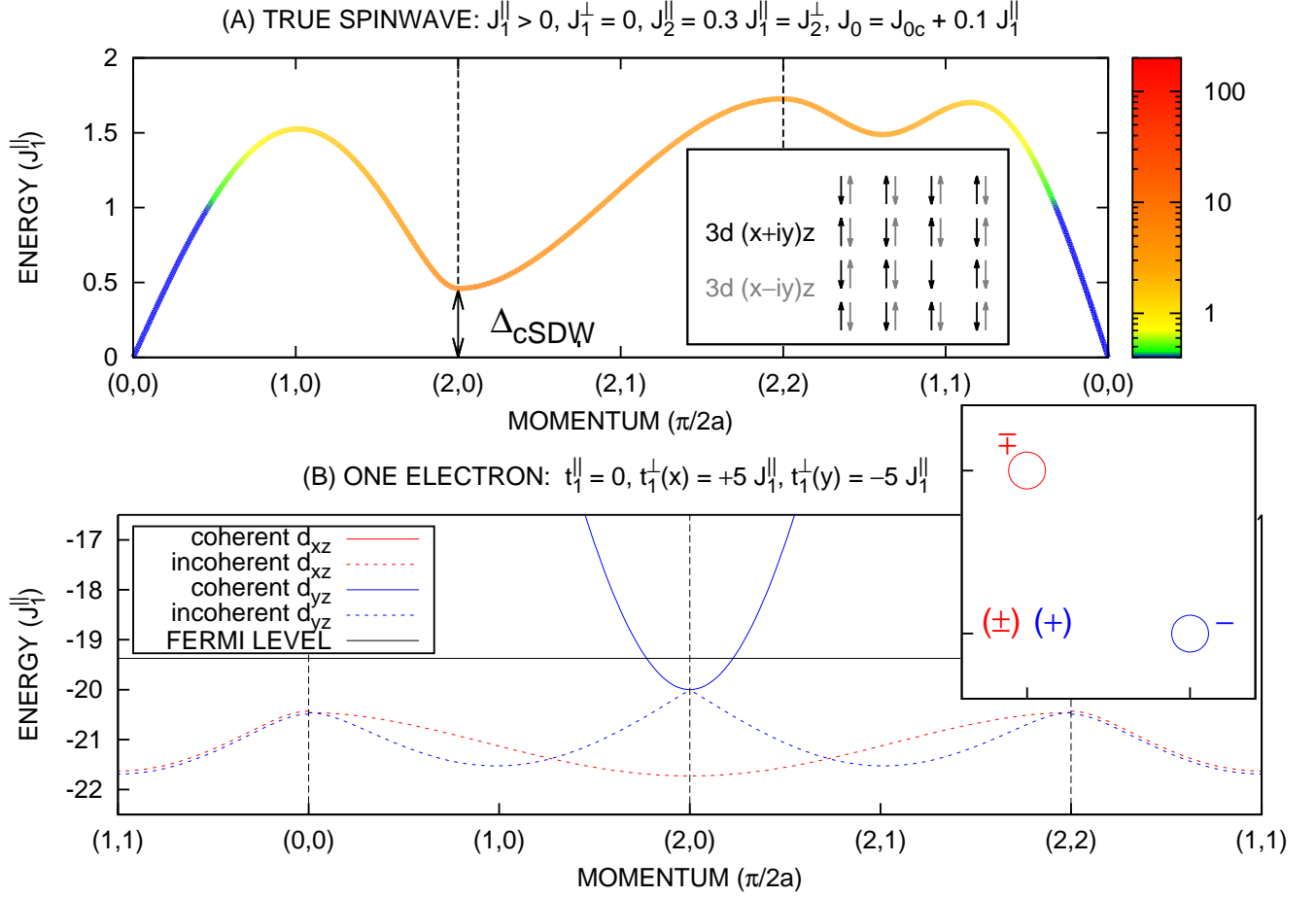


FIG. 1: (a) The imaginary part of the transverse spin susceptibility, Eq. 3, in the true spin channel and (b) the imaginary part of the one-electron propagator near half filling, Eq. 5, at site-orbital concentration  $x = 0.01$ . Not shown in (b) is intrinsic broadening due to the incoherent contributions in Eq. 4.

orbital and by electron-type Fermi surface pockets (inset to Fig. 1b). Emergent hole bands at wavenumber  $(\pi/a)(\hat{x} + \hat{y})$  in the one-iron Brillouin zone are also predicted, but they lie below the former ones in energy. It is important to point out that one-electron tight-binding models that include  $d_{xz}$ ,  $d_{yz}$ , and up to  $d_{xy}$  iron orbitals are unable to account for buried hole bands at the center *and* at the corner of the one-iron Brillouin zone. (Cf. refs. [25] and [26].) Last, exact calculations of two mobile electrons in the two-orbital  $t$ - $J$  model find evidence for isotropic Cooper pairs on both the electron pockets and on the emergent hole bands below the Fermi level as Hund coupling approaches a quantum critical point (QCP) at which commensurate spin-density wave (cSDW) nesting begins. The sign of the Cooper pair wavefunction notably alternates between the electron and hole bands[27, 28].

*Local Moment Model.* Our starting point is a two-orbital  $t$ - $J$  model over the square lattice, where the on-site-orbital energy cost  $U_0$  tends to infinity[29, 30]:

$$H = \sum_{\langle i,j \rangle} [-(t_1^{\alpha,\beta} \tilde{c}_{i,\alpha,s}^\dagger \tilde{c}_{j,\beta,s} + \text{h.c.}) + J_1^{\alpha,\beta} \mathbf{S}_{i,\alpha} \cdot \mathbf{S}_{j,\beta}] + \sum_{\langle\langle i,j \rangle\rangle} J_2^{\alpha,\beta} \mathbf{S}_{i,\alpha} \cdot \mathbf{S}_{j,\beta} + \sum_i (J_0 \mathbf{S}_{i,d-} \cdot \mathbf{S}_{i,d+} + U'_0 \bar{n}_{i,d+} \bar{n}_{i,d-}). \quad (1)$$

Above,  $\mathbf{S}_{i,\alpha}$  is the spin operator that acts on spin  $s_0 = 1/2$  states of  $d- = d_{(x-iy)z}$  and  $d+ = d_{(x+iy)z}$  orbitals  $\alpha$  in iron atoms at sites  $i$ . Repeated orbital and spin indices in the hopping and Heisenberg exchange terms above are summed over. Nearest neighbor and next-nearest neighbor Heisenberg exchange across the links  $\langle i,j \rangle$  and  $\langle\langle i,j \rangle\rangle$  is controlled by exchange coupling constants  $J_1^{\alpha,\beta}$  and  $J_2^{\alpha,\beta}$ , respectively. Hopping of an electron in orbital  $\alpha$  to a nearest-neighbor orbital  $\beta$  is controlled by the matrix element  $t_1^{\alpha,\beta}$ . We adopt the Schwinger-boson ( $b$ ) slave-fermion ( $f$ ) representation for the creation operator of the correlated electron[31–33] at or *above* half filling:  $\tilde{c}_{i,\alpha,s}^\dagger = f_{i,\alpha}^\dagger b_{i,\alpha,s}$  with the constraint

$$2s_0 = b_{i,\alpha,\uparrow}^\dagger b_{i,\alpha,\uparrow} + b_{i,\alpha,\downarrow}^\dagger b_{i,\alpha,\downarrow} + f_{i,\alpha}^\dagger f_{i,\alpha} \quad (2)$$

enforced at each site-orbital to impose the  $U_0 \rightarrow \infty$  limit on electrons with spin  $s_0 = 1/2$ . Finally,  $J_0$  is a ferromagnetic exchange coupling constant that imposes Hund's Rule, while the last term in (1) represents the additional energy cost of a fully occupied iron atom. Here  $\bar{n}_{i,\alpha} = \sum_s \tilde{c}_{i,\alpha,s}^\dagger \tilde{c}_{i,\alpha,s} - 1$  counts singlet pairs at site-orbitals. Last, notice that  $d\pm \rightarrow e^{\pm i\theta} d\pm$  is equivalent to a rotation of the orbitals by an angle  $\theta$  about the  $z$  axis. Spin and occupation operators remain invariant under it. Magnetism described by the two-orbital  $t$ - $J$  model (1) is hence isotropic, which suppresses orbital order.

Semi-classical calculations of the Heisenberg model that corresponds to (1) at half filling find a QCP that separates a cSDW at strong Hund coupling from a hidden antiferromagnet at weak Hund coupling when diagonal frustration is present[34]: e.g.  $J_1^\parallel > 0$ ,  $J_1^\perp = 0$ , and  $J_2^\parallel = J_2^\perp > 0$ . Here,  $\parallel$  and  $\perp$  represent intra-orbital ( $d \pm d\pm$ ) and inter-orbital ( $d \pm d\mp$ ) superscripts. The hidden-order magnet shows Néel spin order per  $d\pm$  orbital following the inset to Fig. 1a. Ideal hopping of electrons within an antiferromagnetic sublattice,  $t_1^\parallel = 0$  and  $t_1^\perp(\hat{\mathbf{x}}) = -t_1^\perp(\hat{\mathbf{y}}) > 0$ , leaves such hidden magnetic order intact in the semi-classical limit,  $s_0 \rightarrow \infty$ . Below, we employ a mean-field approximation of (1) and (2) to study this state near the QCP. It reveals a half metal with circular Fermi surface pockets at wavenumbers  $(\pi/a)\hat{\mathbf{x}}$  and  $(\pi/a)\hat{\mathbf{y}}$ , for electrons in the  $d_{yz}$  orbital and  $d_{xz}$  orbital, respectively.

*Spin-Fluctuations, One-Electron Spectrum.* Following Arovas and Auerbach[31], we first rotate the spins quantized along the  $z$  axis on *one* of the antiferromagnetic sublattices shown in the inset to Fig. 1a by an angle  $\pi$  about the  $y$  axis. This decouples the up and down spins between the two sublattices[35]. We next define mean fields that are set by the pattern of antiferromagnetic versus ferromagnetic pairs of neighboring spins[31] in the hidden magnetic order:  $Q_0 = \langle b_{i,d-,s} b_{i,d+,s} \rangle$ ,  $Q_1^\parallel = \langle b_{i,d\pm,s} b_{j,d\pm,s} \rangle$  and  $Q_2^\perp = \langle b_{i,d\pm,s} b_{j,d\mp,s} \rangle$  on the antiferromagnetic links versus  $Q_1^\perp = \langle b_{i,d\pm,s}^\dagger b_{j,d\mp,s} \rangle$  and  $Q_2^\parallel = \langle b_{i,d\pm,s}^\dagger b_{j,d\pm,s} \rangle$  on the ferromagnetic links of the hidden Néel state. Subscripts 0, 1 and 2 represent on-site, nearest neighbor and next-nearest neighbor links. We add to that list the mean field  $P_1^\perp = \frac{1}{2} \langle f_{i,d\pm}^\dagger f_{j,d\mp} \rangle$  for nearest-neighbor hopping of electrons across the two orbitals. It has  $d$ -wave symmetry. The corresponding mean-field approximation for the  $t$ - $J$  model Hamiltonian (1) then has the form  $H_b + H_f$ , where

$$H_b = \frac{1}{2} \sum_k \sum_s \{ \Omega_{fm}(k) [b_s^\dagger(k) b_s(k) + b_s(-k) b_s^\dagger(-k)] + \Omega_{afm}(k) [b_s^\dagger(k) b_s^\dagger(-k) + b_s(-k) b_s(k)] \}$$

is the Hamiltonian for free Schwinger bosons, and where  $H_f = \sum_k \varepsilon_f(k) f^\dagger(k) f(k)$  is the Hamiltonian for free slave fermions. Here,  $k = (k_0, \mathbf{k})$  is the 3-momentum for these excitations, where the quantum numbers  $k_0 = 0$  and  $\pi$  represent even and odd superpositions of the  $d-$  and  $d+$  orbitals:  $d_{xz}$  and  $(-i)d_{yz}$ .

Enforcing the infinite- $U_0$  constraint (2) on average over the bulk then results in ideal Bose-Einstein condensation (BEC) of the Schwinger bosons into degenerate groundstates at  $k = 0$  and  $(\pi, \pi/a, \pi/a)$  in the zero-temperature limit:  $\langle b_{i,d\pm,s} \rangle = s_0^{1/2}$  at large  $s_0$ . (See Fig. 1a and supplemental Fig. S1.) In such case, all five mean fields among the Schwinger bosons therefore take on the unique value  $Q = s_0$  [35]. This results in diagonal and off-diagonal Hamiltonian matrix elements

$$\begin{aligned} \Omega_{fm}(k) &= (1-x)^2 s_0 (J_0 + 4J_1^\parallel + 4J_2^\perp \\ &\quad - 4J_1^{\prime\perp} [1 - e^{ik_0} \gamma_{1+}(\mathbf{k})] - 4J_2^\parallel [1 - \gamma_2(\mathbf{k})]) \\ \Omega_{afm}(k) &= -(1-x)^2 s_0 [J_0 e^{ik_0} + 4J_1^\parallel \gamma_{1+}(\mathbf{k}) + 4J_2^\perp e^{ik_0} \gamma_2(\mathbf{k})] \end{aligned}$$

for free Schwinger bosons, and the energy eigenvalues  $\varepsilon_f(k) = -8s_0 t_1^\perp(\hat{\mathbf{x}}) e^{ik_0} \gamma_{1-}(\mathbf{k})$  for free slave fermions. Above,  $J_1^{\prime\perp} = J_1^\perp - 2t_1^\perp(\hat{\mathbf{x}}) P_1^\perp(\hat{\mathbf{x}})/(1-x)^2 s_0$ , while  $\gamma_{1\pm}(\mathbf{k}) = \frac{1}{2}(\cos k_x a \pm \cos k_y a)$  and  $\gamma_2(\mathbf{k}) = \frac{1}{2}(\cos k_+ a + \cos k_- a)$ , with  $k_\pm = k_x \pm k_y$ . Slave fermions in  $d_{xz}$  and  $d_{yz}$  orbitals lie within circular Fermi surfaces centered at wavenumbers  $(\pi/a)\hat{\mathbf{y}}$  and  $(\pi/a)\hat{\mathbf{x}}$ ,

respectively, with Fermi wave vector  $k_F a = (4\pi x)^{1/2}$  at low electron doping per iron orbital,  $x \ll 1$ . (See the inset to Fig. 1b.) The mean inter-orbital electron hopping amplitude is then approximately  $P_1^\perp(\hat{\mathbf{x}}) = x/2$ .

The dynamical spin correlation function  $\langle S_y S'_y \rangle$  is obtained directly from the above Schwinger-boson-slave-fermion mean field theory. It is given by an Auerbach-Arovas expression at non-zero temperature that is easily evaluated in the zero-temperature limit [30, 36], where ideal BEC of the Schwinger bosons into the degenerate groundstates at 3-momenta  $k = 0$  and  $(\pi, \pi/a, \pi/a)$  occurs. It is one half the transverse spin correlator, which under ideal BEC and at large  $s_0$  reads

$$i\langle S^{(+)} S'^{(-)} \rangle|_{k,\omega} = (1-x)^2 s_0 (\Omega_+/\Omega_-)^{1/2} ([\omega_b(k) - \omega]^{-1} + [\omega_b(k) + \omega]^{-1}). \quad (3)$$

Here,  $\omega_b = (\Omega_{fm}^2 - \Omega_{afm}^2)^{1/2}$  is the energy dispersion of the Schwinger bosons, and  $\Omega_\pm = \Omega_{fm} \pm \Omega_{afm}$ . Figure 1a depicts the imaginary part of the transverse susceptibility (3) in the true spin channel,  $k_0 = 0$ , at sub-critical Hund coupling. It reveals a spin gap at cSDW wave numbers  $(\pi/a)\hat{\mathbf{x}}$  and  $(\pi/a)\hat{\mathbf{y}}$  of the form  $\Delta_{cSDW} = (1-x)^2 (2s_0)(4J_2^\perp - J_{0c})^{1/2} \text{Re}(J_0 - J_{0c})^{1/2}$ . Here,  $-J_{0c} = 2(J_1^\parallel - J_1^\perp) - 4J_2^\parallel + (1-x)^{-2} s_0^{-1} 2t_1^\perp(\hat{\mathbf{x}})x$  is the critical Hund coupling at which  $\Delta_{cSDW} \rightarrow 0$ . Notice that inter-orbital hopping stabilizes the hidden half metal state. The autocorrelator of the hidden spin  $\mathbf{S}_{i,d-} - \mathbf{S}_{i,d+}$ , (3) at  $k_0 = \pi$ , also shows the above spin gap at cSDW momenta,  $\Delta_{cSDW}$ , in addition to a hidden-order Goldstone mode at Néel wavenumber  $(\pi/a)(\hat{\mathbf{x}} + \hat{\mathbf{y}})$ [35].

The electronic structure of the hidden half metal state can also be obtained directly from the above Schwinger-boson-slave-fermion mean field theory. In particular, the one-electron propagator is given by the convolution of the conjugate propagator for Schwinger bosons with the propagator for slave fermions in 3-momentum and in frequency. A summation of Matsubara frequencies yields the expression[35]

$$G(k, \omega) = \frac{1}{\mathcal{N}} \sum_q \left[ \left( \frac{1}{2} \frac{\Omega_{fm}}{\omega_b} \right) \Big|_{q-k} + \frac{1}{2} \right) \frac{n_B[\omega_b(q-k)] + n_F[\varepsilon_f(q) - \mu]}{\omega + \omega_b(q-k) - \varepsilon_f(q) + \mu} + \left( \frac{1}{2} \frac{\Omega_{fm}}{\omega_b} \right) \Big|_{q-k} - \frac{1}{2} \right) \frac{n_B[\omega_b(q-k)] + n_F[\mu - \varepsilon_f(q)]}{\omega - \omega_b(q-k) - \varepsilon_f(q) + \mu} \Big]. \quad (4)$$

Above,  $n_B$  and  $n_F$  denote the Bose-Einstein and the Fermi-Dirac distributions, and  $\mu$  denotes the chemical potential of the slave fermions. Ideal BEC of the Schwinger bosons at 3-momenta  $q - k = 0$  and  $(\pi, \pi/a, \pi/a)$  results in the following coherent contribution to the

electronic spectral function at zero temperature and at large  $s_0$ :  $\text{Im } G_{\text{coh}}(k, \omega) = s_0 \pi \delta[\omega + \mu - \varepsilon_f(k)]$ . It reveals degenerate electron bands for  $d_{xz}$  and  $d_{yz}$  orbitals centered at cSDW wave numbers  $\mathbf{Q}_0 = (\pi/a)\hat{\mathbf{y}}$  and  $\mathbf{Q}_\pi = (\pi/a)\hat{\mathbf{x}}$ , respectively. The electron Fermi surface pockets at  $\omega = 0$  are depicted by the inset to Fig. 1b. At energies below the Fermi level,  $\omega < 0$ , the remaining contribution is exclusively due to the first fermion term in (4). Inspection of Fig. 1b (solid lines) yields the following expression for it in the limit near half-filling,  $k_F a \rightarrow 0$ , at large  $t/J$  [37]:

$$\text{Im } G_{\text{inc}}(k, \omega) \cong \sum_{q_0=0,\pi} \frac{\pi}{2} x \left[ \frac{1}{2} + \frac{1}{2} \frac{\Omega_{fm}}{\omega_b} \Big|_{(q_0-k_0, \mathbf{Q}_{q_0}-\mathbf{k})} \right] \delta[\omega + \epsilon_F + \omega_b(q_0 - k_0, \mathbf{Q}_{q_0} - \mathbf{k})]. \quad (5)$$

Figure 1b displays the emergent hole bands predicted above. They lie  $\epsilon_F + \Delta_{\text{cSDW}}$  below the Fermi level, with degenerate maxima at  $\mathbf{k} = 0$  and  $(\pi/a)(\hat{\mathbf{x}} + \hat{\mathbf{y}})$ . Here,  $\epsilon_F = (2s_0)t_1^\perp(\hat{\mathbf{x}})(k_F a)^2$  is the Fermi energy. The emergent hole bands also show intrinsic broadening in frequency at zero temperature, which makes them incoherent. Outside the critical region, at large  $t/J$ , the broadening is  $\Delta\omega \sim k_F |\nabla \omega_b|_{\mathbf{Q}-\mathbf{k}}$ . It remains small at the previous maxima [38]. Last, the emergent hole bands predicted by (5) are anisotropic: e.g., the  $d_{yz}$  hole band at zero 2D momentum has mass anisotropy  $|m_x| < |m_y|$ . (Cf. ref. [39].)

Adding intra-orbital electron hopping,  $t_1^\parallel > 0$ , brings the emergent hole bands at wavenumber  $(\pi/a)(\hat{\mathbf{x}} + \hat{\mathbf{y}})$  down in energy below the ones at zero 2D momentum. This is confirmed by exact calculations of the two-orbital  $t$ - $J$  model with one electron more than half filling over a  $4 \times 4$  lattice of iron atoms under periodic boundary conditions. The previous Schwinger-boson-slave-fermion description (2) for spin  $s_0 = 1/2$  electrons is exploited to impose strong on-site-orbital Coulomb repulsion. Details are given in ref. [30]. Figure 2a shows the exact spectrum at the QCP, where  $\Delta_{\text{cSDW}} \rightarrow 0$ . The  $t$ - $J$  model parameters coincide with those set by Fig. 1, but with  $t_1^\parallel = 2J_1^\parallel$ , and with Hund coupling tuned to the critical value  $-J_0 = 1.733J_1^\parallel$ . Red states have even parity under orbital swap,  $P_{d,\bar{d}}$ , while blue states have odd parity under it. Notice that the lowest-energy doubly-degenerate states at wave number  $(\pi/a)(\hat{\mathbf{x}} + \hat{\mathbf{y}})$ , which are spin-1/2, lie  $0.5J_1^\parallel$  in energy above the doubly-degenerate spin-1/2 groundstates at zero 2D momentum. The latter states (purple) move up in energy off the Fermi level set by the groundstates at cSDW momenta as Hund coupling falls below the critical value, and they become nearly degenerate with the former states in the absence of Hund's Rule. This dependence on Hund coupling is demonstrated by the inset to Fig. 2a and by supplemental Fig. S3. The exact low-energy spectrum at

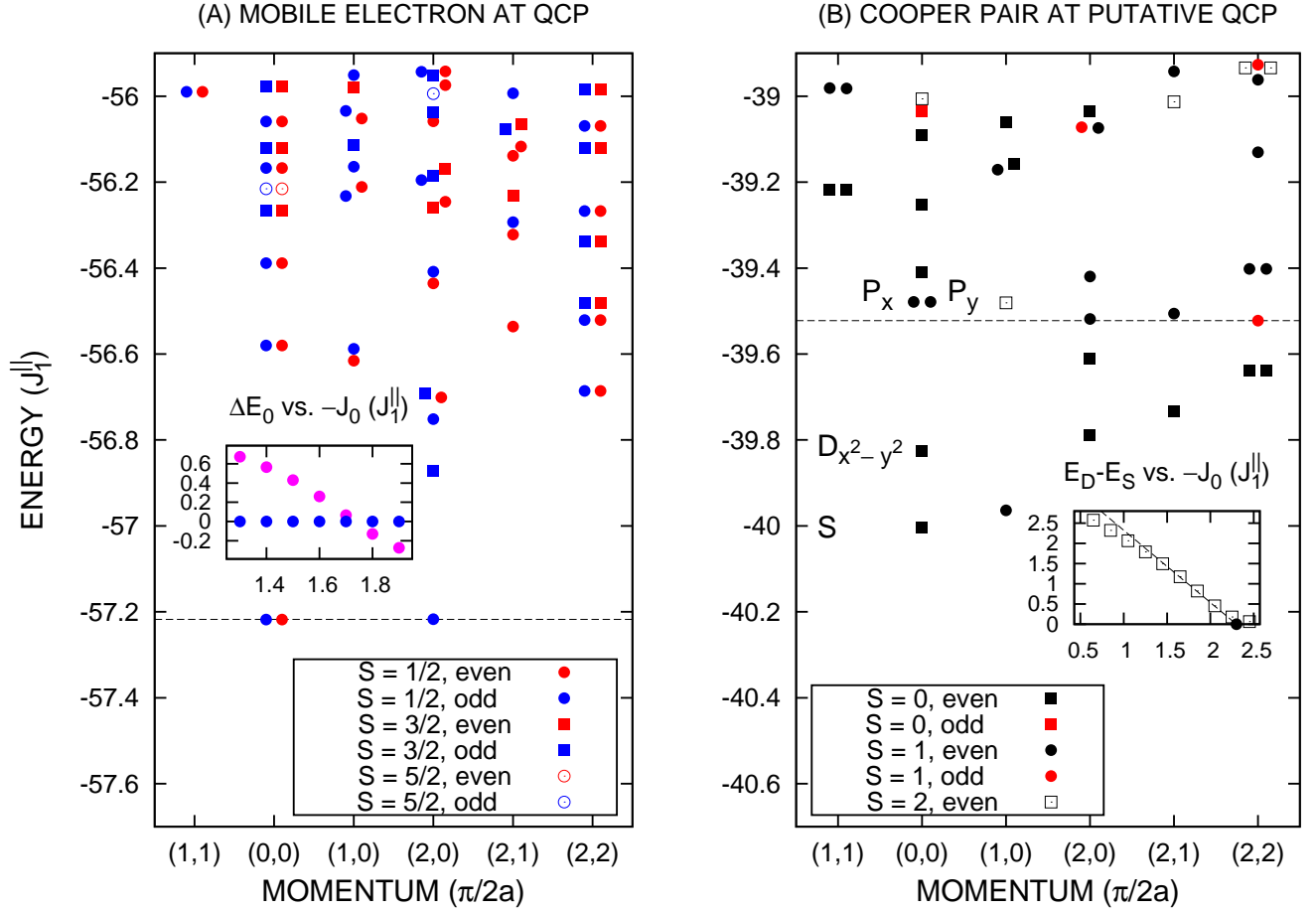


FIG. 2: (a) Low-energy spectrum of two-orbital  $t$ - $J$  model, Eq. (1) plus constant  $\frac{3}{4}(N_{\text{Fe}} - 1)J_0$ , over a  $4 \times 4$  lattice, with one electron more than half filling. Model parameters coincide with those listed by Fig. 1, except  $t_1^\parallel = 2J_1^\parallel$  and  $-J_0 = 1.733J_1^\parallel$ . (b) Low-energy spectrum of Eq. (1) plus repulsive interactions (see text) plus constant  $\frac{1}{4}(N_{\text{Fe}} - 2)J_0$ , but with two electrons more than half filling, with  $-J_0 = 2.25J_1^\parallel$ , and with  $U'_0 = \frac{1}{4}J_0 + 1000J_1^\parallel$ . Some points in spectra are artificially moved slightly off their quantized values along the momentum axis for the sake of clarity.

sub-critical Hund coupling is therefore consistent with the emergent hole bands obtained by the meanfield approximation, Fig. 1b, but with the hole bands centered at wavenumber  $(\pi/a)(\hat{x} + \hat{y})$  pulled down to lower energy. Last, Fig. 2a shows that the even parity ( $d_{xz}$ ) and odd parity ( $d_{yz}$ ) spin-1/2 groundstates at wavenumber  $(\pi/2a)\hat{x}$  are nearly degenerate, which suggests isotropic emergent hole bands at zero 2D momentum near the QCP.

*Cooper Pairs.* Figure 2b shows the spectrum of the same two-orbital  $t$ - $J$  model (1), but with two electrons more than half filling. A *repulsive* interaction has been added to the Heisenberg exchange terms in order to reduce finite-size effects:  $\mathbf{S}_{i,\alpha} \cdot \mathbf{S}_{j,\beta} \rightarrow \mathbf{S}_{i,\alpha} \cdot \mathbf{S}_{j,\beta} +$



$\frac{1}{4}n_{i,\alpha}n_{j,\beta}$ , equal to  $1/2$  the spin-exchange operator. Here,  $n_{i,\alpha}$  counts the net occupation of *holes* per site-orbital. Also, the on-site repulsion between mobile electrons in the  $d+$  and  $d-$  orbitals, respectively, is set to a large value  $U'_0 = \frac{1}{4}J_0 + 1000 J_1^\parallel$ . The Schwinger-boson-slave-fermion description of the correlation electron (2) is again employed, with  $s_0 = 1/2$ . Details are given in ref. [40]. Last, the ferromagnetic Hund's Rule exchange coupling constant is tuned to the critical value  $J_0 = -2.25 J_1^\parallel$ , at which  $\Delta_{cSDW} \rightarrow 0$ . This is depicted by the dashed horizontal line in Fig. 2b, which shows the degeneracy between the cSDW spin resonance at wavenumber  $(\pi/a)\hat{\mathbf{x}}$  with the hidden-order spin resonance at wavenumber  $(\pi/a)(\hat{\mathbf{x}} + \hat{\mathbf{y}})$ . The former is even (black) under swap of the orbitals,  $d- \leftrightarrow d+$ , while latter is odd (red) under it. Notice that the groundstate and the second excited state both lie under a continuum of states at zero net momentum. They respectively have even and odd parity under a reflection about the  $x$ - $y$  diagonal. We therefore assign  $S$  symmetry to the groundstate bound pair and  $D_{x^2-y^2}$  symmetry to the excited-state bound pair. The dependence of the energy-splitting between these two states on Hund coupling is shown by the inset to Fig. 2b. It provides evidence for a true QCP in the thermodynamic limit at  $-J_0 = 2.30 J_1^\parallel$ , where the  $s$ -wave and  $d$ -wave bound states become degenerate.

Figure 3 depicts the order parameters for superconductivity of the two bound pair states shown in Fig. 2b:

$$iF(k_0, \mathbf{k}) = \langle \Psi_{\text{Mott}} | \tilde{c}_\uparrow(k_0, \mathbf{k}) \tilde{c}_\downarrow(k_0, -\mathbf{k}) | \Psi_{\text{Cooper}} \rangle \quad (6)$$

times  $\sqrt{2}$ , with  $\tilde{c}_s(k_0, \mathbf{k}) = \mathcal{N}^{-1/2} \sum_i \sum_{\alpha=0,1} e^{-i(k_0\alpha + \mathbf{k} \cdot \mathbf{r}_i)} \tilde{c}_{i,\alpha,s}$ . Here,  $\langle \Psi_{\text{Mott}} |$  denotes the critical antiferromagnetic state of the corresponding Heisenberg model[34] at  $-J_{0c} = 1.35 J_1^\parallel$ . (See supplemental Fig. S4.) The groundstate has  $S$  symmetry, as expected, but it also alternates in sign between Cooper pairs at electron Fermi surface pockets versus Cooper pairs at the emergent hole bands. (See Fig. 1b.) Figure 3 also shows that the (second) excited state has  $D_{x^2-y^2}$  symmetry, as expected, and that it alternates in sign in a similar way. The present exact results therefore provide evidence for remnant pairing on the emergent hole bands that lie below the Fermi level at zero 2D momentum.

*Discussion and Conclusions.* The electronic structure in single-layer FeSe/STO is qualitatively described by the combination of Figs. 1b and 2a. For example, a fit of inelastic neutron scattering data in iron-pnictide superconductors to the true linear spinwave spectrum Fig. 1a, but at the QCP, yields  $J_1^\parallel \cong 110$  meV,  $J_1^\perp = 0$ , and  $J_2^\parallel \cong 40$  meV  $\cong J_2^\perp$  for the Heisenberg exchange coupling constants[34]. Hopping parameters set in Figs. 1b and 2a

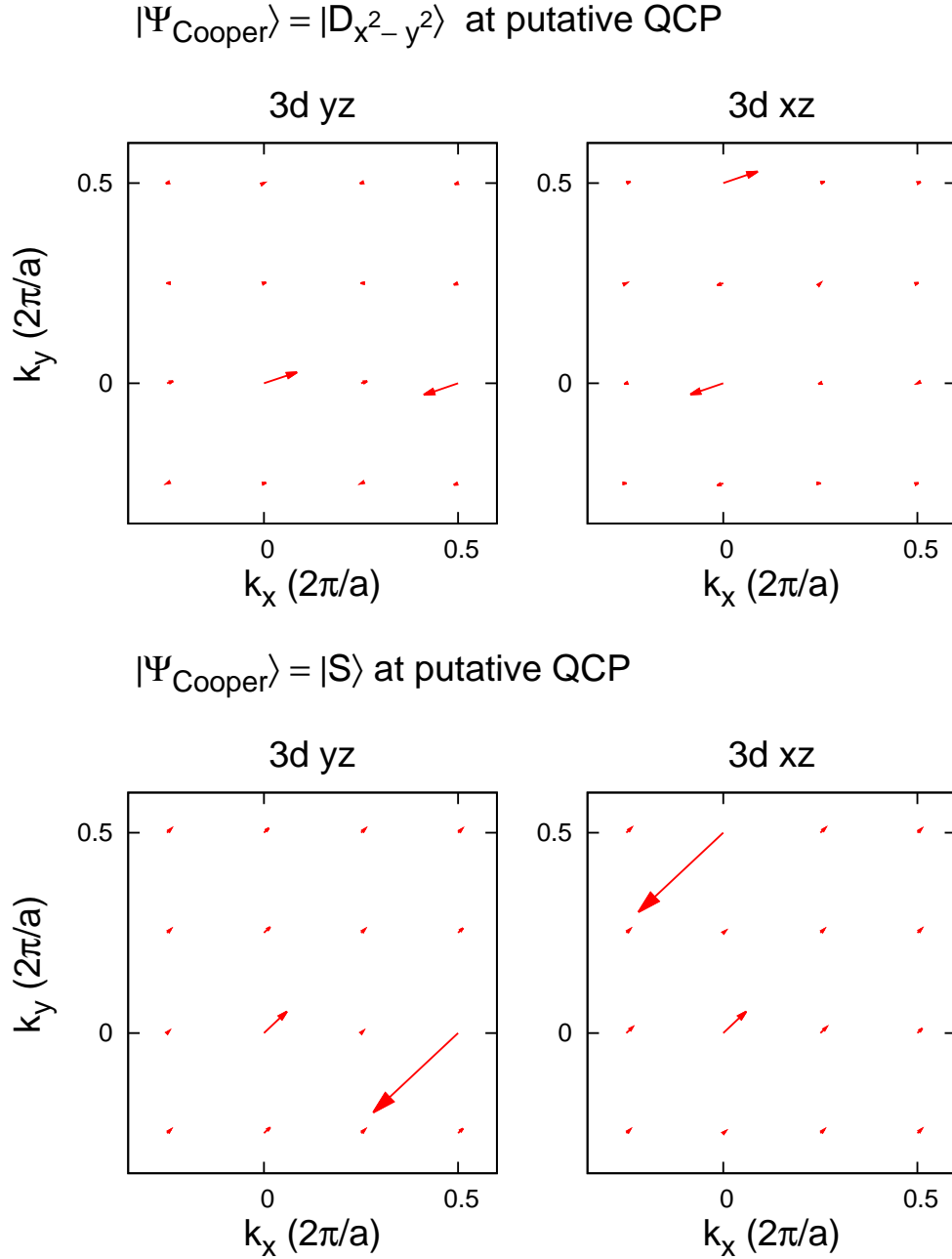


FIG. 3: The complex order parameter for superconductivity, Eq. 6, symmetrized with respect to both reflections about the principal axes.

imply that the bottom of the electron bands lies  $\epsilon_F \cong 60$  meV below the Fermi level. Also, the cSDW spin gap displayed by Fig. 1a at sub-critical Hund coupling is approximately 50 meV, which therefore implies that the emergent hole bands at zero 2D momentum lie 110 meV below the Fermi. Both energy levels are roughly consistent with ARPES in single-layer

FeSe/STO[6]. Last, the mean-field and exact spectra displayed by Figs. 1b and 2a predict that “replicas” of the  $d_{xz}/d_{yz}$  buried hole bands exist at the corner of the one-iron Brillouin zone, but with orbital quantum numbers interchanged and at lower energy. A substrate leads to two inequivalent iron atoms per hopping of electrons in  $d_{xz}$  and  $d_{yz}$  orbitals to neighboring sites. Zone-folding of the “replica” bands at lower energy to the center of the two-iron Brillouin zone possibly accounts for the “ $D'$  replicas” of the buried hole bands that are observed by ARPES on FeSe/STO[9].

Figure 3 predicts  $s$ -wave Cooper pairs on the electron Fermi surface pockets at cSDW momenta. This is consistent with ARPES and with STM on heavily electron-doped surfaces of FeSe, which find a gap on the electron Fermi surface pockets, and no evidence for nodes[8, 10, 11, 13, 16, 17]. Notably absent from our local moment model (1) is the  $3d_{xy}$  electron orbital of the iron atom. DFT calculations predict inner and outer electron Fermi surface pockets at the corner of the two-iron Brillouin zone that have  $d_{xz}/d_{yz}$  and  $d_{xy}$  orbital character, respectively[20]. In such case, the limit of strong on-site Coulomb repulsion assumed here would require remnant  $s$ -wave pairing of opposite sign on the buried  $d_{xy}$  band at the center of the Brillouin zone. The spectral weight of this band is negligibly small compared to that of the buried  $d_{xz}/d_{yz}$  hole bands according to high-resolution ARPES on alkali-metal doped FeSe[16], however. This contradiction argues that the iron  $3d_{xy}$  orbital does not play an important role in high-temperature superconductivity shown at surface layers of heavily electron-doped FeSe.

Figure 3 also predicts remnant Cooper pairs of opposite sign on the emergent hole bands that lie below the Fermi level at zero 2D momentum. The remnant pairs are possibly a result of the intrinsic broadening in frequency experienced by the emergent holes. (Cf. ref. [41].) Recent quasi-particle interference patterns obtained from surface layers of intercalated FeSe observe a feature at cSDW wavenumbers that could be accounted for by the superposition of an electron near cSDW momenta with an Andreev reflected hole near zero 2D momentum[13]. Remnant hole pairing can be confirmed in this way.

*Note added:* Recent inelastic neutron scattering studies of intercalated FeSe find low-energy spin resonances in the superconducting state at wavenumbers  $\mathbf{Q} = (\pi/a)(\hat{\mathbf{x}} + \hat{\mathbf{y}}) \pm \delta(\pi/a)\hat{\mathbf{x}}(\hat{\mathbf{y}})$  in the one-iron Brillouin zone[42], with  $\delta = 0.32 - 0.47$ . Comparison of Fig. 1a with supplemental Fig. S1 reveals that true spin waves become degenerate with hidden spin waves precisely at such wavenumbers ( $\delta = 0.36$ ). This observation suggests that hidden

magnetic order of the type displayed in the inset to Fig. 1a is present in intercalated FeSe.

The author thanks Nick Bonesteel, Pedro Schlottmann and Oskar Vafeek for discussions. He also thanks Brent Andersen, Richard Roberts and Timothy Sell for technical help with the use of the shared-memory machine (Predator) at the AFRL DoD Supercomputing Resource Center. This work was supported in part by the US Air Force Office of Scientific Research under grant no. FA9550-13-1-0118 and by the National Science Foundation under PREM grant no. DMR-1523588.

- 
- [1] Y. Kamihara, T. Watanabe, M. Hirano, and H. Hosono, J. Am. Chem. Soc. **130**, 3296 (2008).
  - [2] Q.-Y. Wang, Z. Li, W.-H. Zhang, Z.-C. Zhang, J.-S. Zhang, W. Li, H. Ding, Y.-B. Ou, P. Deng, K. Chang, J. Wen, C.-L. Song, K. He, J.-F. Jia, S.-H. Ji, Y. Wang, L. Wang, X. Chen, X. Ma, Q.-K. Xue, Chin. Phys. Lett. **29**, 037402 (2012).
  - [3] W.-H. Zhang, Y. Sun, J.-S. Zhang, F.-S. Li, M.-H. Guo, Y.-F. Zhao, H.-M. Zhang, J.-P. Peng, Y. Xing, H.-C. Wang, T. Fujita, A. Hirata, Z. Li, H. Ding, C.-J. Tang, M. Wang, Q.-Y. Wang, K. He, S.-H. Ji, X. Chen, J.-F. Wang, Z.-C. Xia, L. Li, Y.-Y. Wang, J. Wang, L.-L. Wang, M.-W. Chen, Q.-K. Xue, and X.-C. Ma, Chin. Phys. Lett. **31**, 017401 (2014).
  - [4] L.Z. Deng, B. Lv, Z. Wu, Y.Y. Xue, W.H. Zhang, F.S. Li, L.L. Wang, X.C. Ma, Q.K. Xue, and C.W. Chu, Phys. Rev. B **90**, 214513 (2014).
  - [5] J.-F. Ge, Z.-L. Liu, C. Liu, C.-L. Gao, D. Qian, Q.-K. Xue, Y. Liu, J.-F. Jia, Nat. Mater. **14**, 285 (2015).
  - [6] D. Liu, W. Zhang, D. Mou, J. He, Y.-B. Ou, Q.-Y. Wang, Z. Li, L. Wang, L. Zhao, S. He, Y. Peng, X. Liu, C. Chaoyu, L. Yu, G. Liu, X. Dong, J. Zhang, C. Chen, Z. Xu, J. Hu, X. Chen, Z. Ma, Q. Xue and X.J. Xhou, Nat. Comm. **3**, 931 (2012).
  - [7] S. He, J. He, W.-H. Zhang, L. Zhao, D. Liu, X. Liu, D. Mou, Y.-B. Ou, Q.-Y. Wang, Z. Li, L. Wang, Y. Peng, Y. Liu, C. Chen, L. Yu, G. Liu, X. Dong, J. Xhang, C. Chen, Z. Xu, X. Chen, X. Ma, Q. Xue, and X.J. Zhou, Nat. Mater. **12**, 605 (2013).
  - [8] R. Peng, X.P. Shen, X. Xie, H.C. Xu, S.Y. Tan, M. Xia, T. Zhang, H.Y. Cao, X.G. Gong, J.P. Hu, B.P. Xie, D. L. Feng, Phys. Rev. Lett. **112**, 107001 (2014).
  - [9] J.J. Lee, F.T. Schmitt, R.G. Moore, S. Johnston, Y.-T. Cui, W. Li, M. Yi, Z.K. Liu, M. Hashimoto, Y. Zhang, D.H. Lu, T.P. Devereaux, D.-H. Lee and Z.-X. Shen, Nature **515**, 245

(2014).

- [10] Q. Fan, W. H. Zhang, X. Liu, Y.J. Yan, M.Q. Ren, R. Peng, H. C. Xu, B. P. Xie, J. P. Hu, T. Zhang, and D. L. Feng, *Nat. Phys.* **11**, 946 (2015).
- [11] L. Zhao, A. Liang, D. Yuan, Y. Hu, D. Liu, J. Huang, S. He, B. Shen, Y. Xu, X. Liu, L. Yu, G. Liu, H. Zhou, Y. Huang, X. Dong, F. Zhou, Z. Zhao, C. Chen, Z. Xu, X.J. Zhou, *Nat. Comm.* **7**, 10608 (2016).
- [12] X.H. Niu, R. Peng, H.C. Xu, Y.J. Yan, J. Jiang, D.F. Xu, T.L. Yu, Q. Song, Z.C. Huang, Y.X. Wang, B.P. Xie, X.F. Lu, N.Z. Wang, X.H. Chen, Z. Sun, and D.L. Feng, *Phys. Rev. B* **92**, 060504(R) (2015).
- [13] Y. J. Yan, W. H. Zhang, M. Q. Ren, X. Liu, X. F. Lu, N. Z. Wang, X. H. Niu, Q. Fan, J. Miao, R. Tao, B. P. Xie, X. H. Chen, T. Zhang, D. L. Feng, *Phys. Rev. B* **94**, 134502 (2016).
- [14] Y. Miyata, K. Nakayama, K. Suawara, T. Sato, and T. Takahashi, *Nat. Mater.* **14**, 775 (2015).
- [15] C.H.P. Wen, H.C. Xu, C. Chen, Z.C. Huang, X. Lou, Y.J. Pu, Q. Song, B.P. Xie, M. Abdel-Hafeez, D.A. Chareev, A.N. Vasiliev, R. Peng, and D.L. Feng, *Nat. Comm.* **7**, 10840, (2016).
- [16] Z.R. Ye, C.F. Zhang, H.L. Ning, W. Li, L. Chen, T. Jia, M. Hashimoto, D.H. Lu, Z.-X. Shen, and Y. Zhang, *arXiv:1512.02526* .
- [17] C.-L. Song, H.-M. Zhang, Y. Zhong, X.-P. Hu, S.-H. Ji, L. Wang, K. He, X.-C. Ma, and Q.-K. Xue, *Phys. Rev. Lett.* **116**, 157001 (2016).
- [18] B. Lei, J.H. Cui, Z.J. Xiang, C. Shang, N.Z. Wang, G.J. Ye, X.G. Luo, T. Wu, Z. Sun, and X.H. Chen, *Phys. Rev. Lett.* **116**, 077002 (2016).
- [19] K. Hanzawa, H. Sato, H. Hiramatsu, T. Kamiya, and H. Hosono, *Proc. Nat. Acad. Sci.* **113**, 3986 (2016).
- [20] O.K. Andersen and L. Boeri, *Annalen der Physik* **523**, 8 (2011).
- [21] T. Bazhiron and M.L. Cohen, *J. Phys.: Condens. Matter* **25**, 105506 (2013).
- [22] J. He, X. Liu, W. Zhang, L. Zhao, D. Liu, S. He, D. Mou, F. Li, C. Tang, Z. Li, L. Wang, Y. Peng, Y. Liu, C. Chen, L. Yu, G. Liu, X. Dong, J. Zhang, C. Chen, Z. Xu, X. Chen, X. Ma, Q. Xue, X. J. Zhou, *Proc. Nat. Acad. Sci.* **111**, 18501 (2014).
- [23] Q. Si and E. Abrahams, *Phys. Rev. Lett.* **101**, 076401 (2008).
- [24] J.P. Rodriguez and E.H. Rezayi, *Phys. Rev. Lett.* **103**, 097204 (2009).
- [25] S. Raghu, Xiao-Liang Qi, Chao-Xing Liu, D.J. Scalapino, Shou-Cheng Zhang, *Phys. Rev. B* **77**, 220503(R) (2008).

- [26] P.A. Lee and X.-G. Wen, Phys. Rev. B **78**, 144517 (2008).
- [27] I.I. Mazin, D.J. Singh, M.D. Johannes, and M.H. Du, Phys. Rev. Lett. **101**, 057003 (2008).
- [28] K. Kuroki, S. Onari, R. Arita, H. Usui, Y. Tanaka, H. Kontani, and H. Aoki, Phys. Rev. Lett. **101**, 087004 (2008).
- [29] J.P. Rodriguez, M.A.N. Araujo, P.D. Sacramento, Phys. Rev. B **84**, 224504 (2011).
- [30] J.P. Rodriguez, M.A.N. Araujo, P.D. Sacramento, Eur. Phys. J. B **87**, 163 (2014).
- [31] D.P. Arovas and A. Auerbach, Phys. Rev. B **38**, 316 (1988).
- [32] C.L. Kane, P.A. Lee and N. Read, Phys. Rev. B **39**, 6880 (1989).
- [33] A. Auerbach and B. E. Larson, Phys. Rev. B **43**, 7800 (1991).
- [34] J.P. Rodriguez, Phys. Rev. B **82**, 014505 (2010).
- [35] See Supplemental Material.
- [36] A. Auerbach and D.P. Arovas, Phys. Rev. Lett. **61**, 617 (1988).
- [37] At wavenumbers  $\mathbf{k} = 0$  and  $(\pi/a)(\hat{\mathbf{x}} + \hat{\mathbf{y}})$ , the spectral weight in (5) diverges as the cSDW spin gap vanishes at the QCP. It yields the bound  $\Delta_{cSDW} > k_F v_0$  that guarantees the validity of (5). Here,  $v_0$  coincides with the velocity of cSDW spinwaves at the QCP[34]. The bound  $|\mathbf{k} - \mathbf{Q}_{q_0}| > k_F$ , likewise, guarantees the validity of (5) at  $\mathbf{k}$  near cSDW wavenumbers  $\mathbf{Q}_{q_0}$ .
- [38] At  $t_1^\parallel = 0$ , the convolution (4) implies intrinsic broadening of the electron bands below the Fermi level:  $\Delta\omega \sim \frac{1}{8}(\epsilon_F/2s_0) = \frac{1}{2}\pi x t_1^\perp(\hat{\mathbf{x}})$  at  $t \gg J$ . The Goldstone mode associated with hidden magnetic order (inset to Fig. 1a) may no longer exist once  $t_1^\parallel \neq 0$ , however. In such case, the coherent and incoherent  $d_{yz}$  bands shown in Fig. 1b may experience level repulsion at cSDW momentum  $(\pi/a)\hat{\mathbf{x}}$ , likewise the  $d_{xz}$  bands at cSDW momentum  $(\pi/a)\hat{\mathbf{y}}$ .
- [39] In the independent electron approximation, adding small but positive intra-orbital nearest-neighbor hopping,  $0 < t_1^\parallel < t_1^\perp(\hat{\mathbf{x}})$ , results in an electron band centered at wavenumber  $(\pi/a)\hat{\mathbf{x}}$  for the  $d_{yz}$  orbital with mass anisotropy  $m_x > m_y$ . The mass anisotropy of the corresponding emergent hole band at zero 2D momentum is the reverse within the Schwinger-boson-slave-fermion mean-field approximation, at ideal hopping,  $t_1^\parallel = 0$ . Adding the mean fields  $R_1^\parallel = \langle b_{i,d\pm,s}^\dagger b_{j,d\pm,s} \rangle$  and  $P_1^\parallel = \frac{1}{2}\langle f_{i,d\pm}^\dagger f_{j,d\pm} \rangle$  for intra-orbital nearest-neighbor hopping of electrons (before any 90 degree spin rotations about the  $y$  axis) results in elliptical electron Fermi surface pockets at wavenumbers  $(\pi/a)\hat{\mathbf{x}}$  and  $(\pi/a)\hat{\mathbf{y}}$  for the  $d_{yz}$  and the  $d_{xz}$  orbitals, respectively, with the major axes along the principal axes. Both of the extra mean fields vanish in the optimized theory at large  $s_0$ , however. (Cf. ref. [30].)

- [40] J.P. Rodriguez, J. Phys.: Condens. Matter **28**, 375701 (2016).
- [41] X. Chen, S. Maiti, A. Linscheid and P.J. Hirschfeld, Phys. Rev. B **92**, 224514 (2015).
- [42] N.R. Davies, M.C. Rahn, H.C. Walker, R.A. Ewings, D.N. Woodruff, S.J. Clarke, and A.T. Boothroyd, Phys. Rev. B **94**, 144503 (2016); B. Pan, Y. Shen, D. Hu, Y. Feng, J.T. Park, A.D. Christianson, Q. Wang, Y. Hao, H. Wo, and J. Zhao, arXiv:1608.01204; M. Ma, L. Wang, P. Bourges, Y. Sidis, S. Danilkin, and Y. Li, Phys. Rev. B **95**, 100504(R) (2017).

# Supplemental Material: Isotropic Cooper Pairs with Emergent Sign Changes in Single-Layer Iron Superconductor

Jose P. Rodriguez

*Department of Physics and Astronomy,  
California State University at Los Angeles, Los Angeles, CA 90032*

## I. SCHWINGER-BOSON-SLAVE-FERMION MEAN FIELD THEORY

It is first convenient to write the spin-operator in the particle-hole-conjugate form:  $\mathbf{S}_{i,\alpha} = -(\hbar/2) \sum_{s,s'} \tilde{c}_{i,\alpha,s} \boldsymbol{\sigma}_{s,s'} \tilde{c}_{i,\alpha,s'}^\dagger$ . Substitution of the composite form for the creation operator of the correlated electron *above* half filling,  $\tilde{c}_{i,\alpha,s}^\dagger = f_{i,\alpha}^\dagger b_{i,\alpha,s}$ , then yields the expression  $\mathbf{S}_{i,\alpha} = -(\hbar/2) \sum_{s,s'} f_{i,\alpha} b_{i,\alpha,s}^\dagger \boldsymbol{\sigma}_{s,s'} b_{i,\alpha,s'} f_{i,\alpha}^\dagger$ . Next, replacing the operator  $f_{i,\alpha} f_{i,\alpha}^\dagger$  with its expectation value,  $1 - x$ , yields the approximation

$$\mathbf{S}_{i,\alpha} \cong -(1-x) \frac{1}{2} \hbar \sum_{s,s'} b_{i,\alpha,s}^\dagger \boldsymbol{\sigma}_{s,s'} b_{i,\alpha,s'} \quad (\text{S1})$$

for the spin operator. Here,  $x$  denotes the concentration of mobile electrons per orbital. Last, we shall also neglect on-site repulsion  $U'_0$  between a mobile electron in the  $d-$  orbital and a mobile electron in the  $d+$  orbital. This approximation should be valid in the dilute limit,  $x \rightarrow 0$ . As mentioned in the paper, it is also convenient to next rotate the spins quantized along the  $z$  axis by an angle  $\pi$  about the  $y$  axis on one of the antiferromagnetic sublattices in the hidden magnetic order shown by the inset to Fig. 1a in the paper; e.g.,  $b_{i,\beta,\uparrow}^\dagger \rightarrow -b_{i,\beta,\downarrow}^\dagger$  and  $b_{i,\beta,\downarrow}^\dagger \rightarrow b_{i,\beta,\uparrow}^\dagger$ , for  $(i, \beta)$  that lie in the down-spin sublattice. This decouples spins between the two hidden antiferromagnetic sublattices[S1].

Let us now turn off nearest-neighbor intra-orbital hopping in the two-orbital  $t$ - $J$  model, Eq. (1) in the paper:  $t_1^\parallel = 0$ . Mean fields among the Schwinger bosons are pair amplitudes across the antiferromagnetic links[S1]:  $Q_0 = \langle b_{i,d-,s} b_{i,d+,s} \rangle$ ,  $Q_1^\parallel = \langle b_{i,d\pm,s} b_{j,d\pm,s} \rangle$  and  $Q_2^\perp = \langle b_{i,d\pm,s} b_{j,d\mp,s} \rangle$ . Here, the superscripts  $\parallel$  and  $\perp$  denote intra-orbital ( $d\pm d\pm$ ) and inter-orbital ( $d\pm d\mp$ ) links, while the subscripts 0, 1 and 2 denote on-site, nearest neighbor and next-nearest neighbor links. On the other hand, mean fields among the Schwinger bosons are hopping amplitudes across the ferromagnetic links[S1]:  $Q_1^\perp = \langle b_{i,d\pm,s}^\dagger b_{j,d\mp,s} \rangle$  and  $Q_2^\parallel = \langle b_{i,d\pm,s}^\dagger b_{j,d\pm,s} \rangle$ . Last, nearest-neighbor hopping of electrons across the two orbitals is



accounted for by the mean field among slave fermions  $P_1^\perp = \frac{1}{2}\langle f_{i,d\pm}^\dagger f_{j,d\mp} \rangle$ , which has  $d$ -wave symmetry:  $P_1^\perp(\hat{\mathbf{y}}) = -P_1^\perp(\hat{\mathbf{x}})$ . The dynamics of free Schwinger bosons is then governed by the Hamiltonian

$$H_b = \frac{1}{2} \sum_k \sum_s \{ \Omega_{fm}(k) [b_s^\dagger(k) b_s(k) + b_s(-k) b_s^\dagger(-k)] + \Omega_{afm}(k) [b_s^\dagger(k) b_s^\dagger(-k) + b_s(-k) b_s(k)] \},$$

with diagonal and off-diagonal matrix elements

$$\begin{aligned} \Omega_{fm}(k) &= \delta\lambda + J'_0 Q_0 + 4J_1^\parallel Q_1^\parallel + 4J_2^\perp Q_2^\perp \\ &\quad - 4[J_1^\perp Q_1^\perp - 2t_1^\perp(\hat{\mathbf{x}}) P_1^\perp(\hat{\mathbf{x}})] [1 - e^{ik_0} \gamma_{1+}(\mathbf{k})] - 4J_2^\parallel Q_2^\parallel [1 - \gamma_2(\mathbf{k})] \\ \Omega_{afm}(k) &= -J'_0 Q_0 e^{ik_0} - 4J_1^\parallel Q_1^\parallel \gamma_{1+}(\mathbf{k}) - 4J_2^\perp Q_2^\perp e^{ik_0} \gamma_2(\mathbf{k}), \end{aligned}$$

while the dynamics of free slave fermions is then governed by the Hamiltonian  $H_f = \sum_k \varepsilon_f(k) f^\dagger(k) f(k)$ , with the energy eigenvalues

$$\varepsilon_f(k) = -8t_1^\perp(\hat{\mathbf{x}}) Q_1^\perp e^{ik_0} \gamma_{1-}(\mathbf{k}).$$

From here on we set  $\hbar = 1$ . Above,  $k = (k_0, \mathbf{k})$  is the 3-momentum for these excitations, with corresponding destruction operators  $b_s(k) = \mathcal{N}^{-1/2} \sum_{\alpha=0}^1 \sum_i e^{-i(k_0\alpha + \mathbf{k}\cdot\mathbf{r}_i)} b_{i,\alpha,s}$  and  $f(k) = \mathcal{N}^{-1/2} \sum_{\alpha=0}^1 \sum_i e^{-i(k_0\alpha + \mathbf{k}\cdot\mathbf{r}_i)} f_{i,\alpha}$ . Here,  $\mathcal{N} = 2N_{\text{Fe}}$  denotes the number of site-orbitals on the square lattice of  $N_{\text{Fe}}$  iron atoms, while the indices 0 and 1 denote the  $d-$  and  $d+$  orbitals  $\alpha$ . The quantum numbers  $k_0 = 0$  and  $\pi$  therefore represent the  $d_{xz}$  and the  $(-i)d_{yz}$  orbitals. Also above,  $\gamma_{1\pm}(\mathbf{k}) = \frac{1}{2}(\cos k_x a \pm \cos k_y a)$  and  $\gamma_2(\mathbf{k}) = \frac{1}{2}(\cos k_+ a + \cos k_- a)$ , with  $k_\pm = k_x \pm k_y$ . The infinite- $U_0$  constraint, Eq. (2) in the paper, is enforced on *average* over the bulk of the system by the boson chemical potential,  $\delta\lambda$ , while the chemical potential of the slave fermions,  $\mu$ , sets the concentration of mobile electrons per site-orbital,  $x$ . Last, the mean-field approximation (S1) that accounts for the effect of mobile electrons on the spin operator results in effective Heisenberg spin-exchange coupling constants[S2]  $J' = (1-x)^2 J$ .

The solution to the above mean field theory is achieved by making the standard Bogoliubov transformation of the boson field[S1]:  $b_s(k) = (\cosh \theta_k) \beta_s(k) + (\sinh \theta_k) \beta_s^\dagger(-k)$ , with  $\cosh 2\theta = \Omega_{fm}/\omega_b$  and  $\sinh 2\theta = -\Omega_{afm}/\omega_b$ , where  $\omega_b = (\Omega_{fm}^2 - \Omega_{afm}^2)^{1/2}$  is the energy of the boson ( $\beta$ ). Enforcing the infinite- $U_0$  constraint [Eq. (2) in the paper] on average then results in ideal Bose-Einstein condensation (BEC) of the Schwinger bosons into degenerate groundstates at  $k = 0$  and  $(\pi, \pi/a, \pi/a)$  as temperature  $T \rightarrow 0$ , in which case  $\delta\lambda \rightarrow 0$ . (See

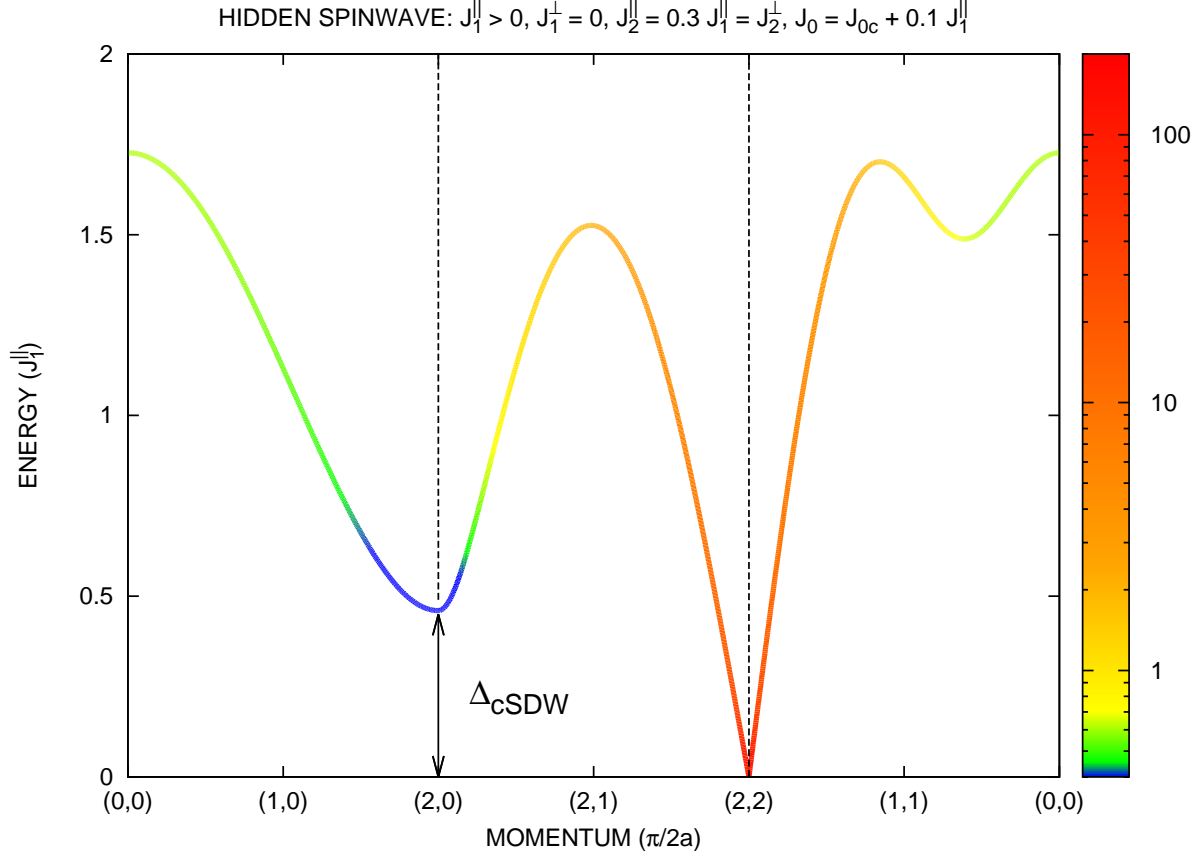


FIG. S1: The imaginary part of the transverse spin susceptibility, Eq. (3) in the paper, at site-orbital concentration  $x = 0.01$ , in the hidden spin channel. Hopping matrix elements are ideal:  $t_1^|| = 0$ ,  $t_1^\perp(\hat{\mathbf{x}}) = +5 J_1^||$ , and  $t_1^\perp(\hat{\mathbf{y}}) = -5 J_1^||$ .

paper, Fig. 1a, and see Fig. S1.) All five mean fields among the Schwinger bosons take on the unique value  $Q = s_0$  at large- $s_0$  under ideal BEC[S3, S4]. Slave fermions in  $d_{xz}$  and  $d_{yz}$  orbitals condense inside of circular Fermi surfaces centered at wavenumbers  $(\pi/a)\hat{\mathbf{y}}$  and  $(\pi/a)\hat{\mathbf{x}}$ , respectively, at low electron doping  $x \ll 1$ , with Fermi wave vector  $k_F a = (4\pi x)^{1/2}$ . (See the inset to Fig. 1b in the paper.) The mean inter-orbital electron hopping amplitude is then approximately  $P_1^\perp(\hat{\mathbf{x}}) = x/2$ .

Equation (3) in the paper for the dynamical spin correlation function  $\langle S^{(+)} S'^{(-)} \rangle|_{k,\omega}$  of the hidden Néel half metal is a direct application of the Auerbach-Arovas expression for the auto-correlation function  $\langle S_y S'_y \rangle|_{k,\omega}$  at ideal BEC of the Schwinger bosons[S4, S5], multiplied by a factor of two because of spin isotropy. The result notably coincides with that obtained within the linear spin-wave approximation at the large- $s_0$  limit[S6]. Figure S1 gives the hidden-order counterpart to the spectrum of true spinwaves near the QCP predicted by this

mean-field approximation, Fig. 1a in the paper. As expected by general considerations[S6], these spectra are shifted with respect to each other by momentum  $(\pi/a)(\hat{\mathbf{x}} + \hat{\mathbf{y}})$ .

Also, within the above mean field theory, the one-electron propagator is given by the convolution of the propagator for slave fermions ( $f$ ) with the conjugate propagator for Schwinger bosons ( $b$ ) in 3-momentum and in frequency:  $iG(k, \omega) = G_b^* * G_f|_{k, \omega}$ . Here, the propagator for free slave fermions reads  $G_f(k, \omega) = [\omega + \mu - \varepsilon_f(k)]^{-1}$ , while the propagator for free Schwinger bosons reads  $G_b(k, \omega) = (\cosh \theta_k)^2 [\omega - \omega_b(k)]^{-1} - (\sinh \theta_k)^2 [\omega + \omega_b(k)]^{-1}$ . The conjugate propagator for free Schwinger bosons evolving backwards in time is then  $G_b^*(k, \omega) = -(\cosh \theta_k)^2 [\omega + \omega_b(k)]^{-1} + (\sinh \theta_k)^2 [\omega - \omega_b(k)]^{-1}$ . After rewriting the resulting products of poles as sums/differences of poles, standard summations of Matsubara frequencies yield expression (4) given in the paper. There, the identities  $(\cosh \theta)^2 = \frac{1}{2} \cosh 2\theta + \frac{1}{2}$  and  $(\sinh \theta)^2 = \frac{1}{2} \cosh 2\theta - \frac{1}{2}$  have been used.

## II. EXACT DIAGONALIZATION

Hidden magnetic order of the type depicted by the inset to Fig. 1a in the paper is predicted by the two-orbital Heisenberg model over the square lattice in the large- $s_0$  limit for exchange coupling constants that exhibit diagonal frustration, at weak to moderate Hund coupling[S6, S7]: e.g.,  $J_1^{\parallel} > 0$ ,  $J_1^{\perp} = 0$ ,  $J_2^{\parallel} = 0.3 J_1^{\parallel} = J_2^{\perp}$ , and  $J_0 = J_{0c} + 0.1 J_1^{\parallel}$ , where  $-J_{0c}$  is the quantum-critical Hund coupling at which the spin gap associated with commensurate spin-density wave (cSDW) order collapses to zero. Add now electrons with ideal nearest-neighbor hopping; e.g.,  $t_1^{\parallel} = 0$ ,  $t_1^{\perp}(\hat{\mathbf{x}}) = +5 J_1^{\parallel}$  and  $t_1^{\perp}(\hat{\mathbf{y}}) = -5 J_1^{\parallel}$ . Spin-polarized electrons hop within each antiferromagnetic sublattice in such case. The critical Hund coupling is given by  $-J_{0c} = 2(J_1^{\parallel} - J_1^{\perp}) - 4J_2^{\parallel} + (1-x)^{-2}s_0^{-1}2t_1^{\perp}(\hat{\mathbf{x}})x$  within the mean-field approximation. Adding mobile electrons thereby stabilizes the hidden Néel order. Figure S1 reveals the Goldstone mode at Néel wavenumber  $(\pi/a)(\hat{\mathbf{x}} + \hat{\mathbf{y}})$  expected from such hidden antiferromagnetic order for the corresponding half metal state of the two-orbital  $t$ - $J$  model within the mean-field approximation[S3, S4]. It appears as a divergence in the imaginary part of the transverse susceptibility, Eq. (3) in the paper, for hidden spin,  $\mathbf{S}_{i,d-} - \mathbf{S}_{i,d+}$ . Recall that spin-1/2 moments live on the  $d\pm = d_{(x\pm iy)z}$  orbitals. The Schwinger-boson-slave-fermion mean-field approximation for the two-orbital  $t$ - $J$  model employed in the paper also predicts coherent electron bands that result in Fermi surface pockets centered at cSDW momenta

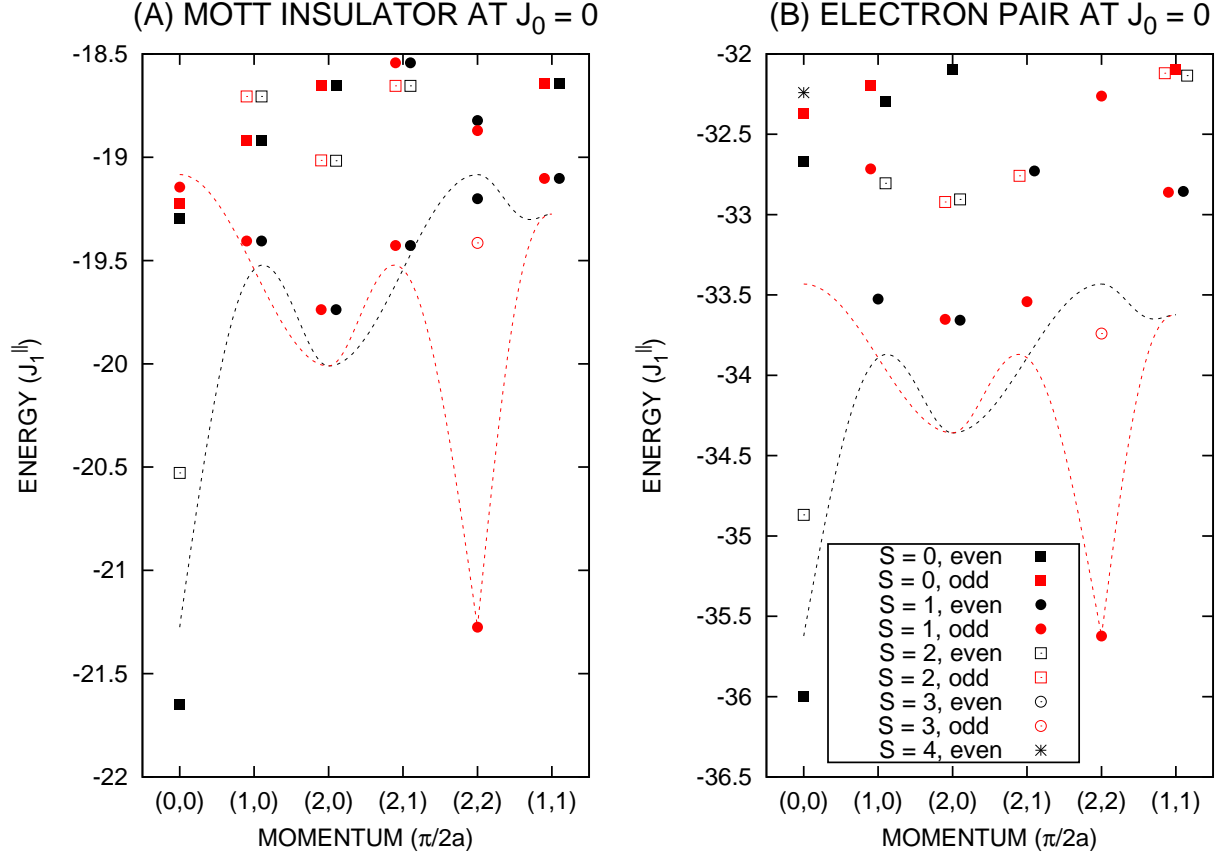


FIG. S2: (a) Exact spectra of two-orbital Heisenberg model over a periodic  $4 \times 4$  lattice, with exchange coupling constants that coincide with those in Fig. S1. Black states are even under orbital exchange,  $P_{d,\bar{d}}$ , while red states are odd under it. Henceforth, some points in spectra are artificially moved slightly off their quantized values along the momentum axis for the sake of clarity. (b) Exact spectrum of two electrons more than half filling for the corresponding two-orbital  $t$ - $J$  model plus repulsive interactions (see paper), plus constant  $\frac{1}{4}(N_{\text{Fe}} - 2)J_0$ . Hopping matrix elements coincide with those in Fig. S3, and  $U'_0 = \frac{1}{4}J_0 + 1000 J_1^{\parallel}$ . In both panels, red and black dashed lines trace the dispersion of hidden and of true spinwaves, respectively, in the limit  $x \rightarrow 0$  following Eq. (3) in the paper.

$(\pi/a)\hat{\mathbf{x}}$  and  $(\pi/a)\hat{\mathbf{y}}$ . (See the inset to Fig. 1b in the paper.) Below, we compare this mean field theory to exact results in the absence of Hund's Rule,  $J_0 = 0$ , where the hidden half metal state is most stable.

*Hund's Rule Absent.* Figure S2a compares exact results for the low-energy spectrum of the frustrated Heisenberg model on a periodic  $4 \times 4$  lattice of iron atoms with  $d-$  and  $d+$  orbitals to the spin-wave spectrum predicted by Schwinger-boson mean field theory for

hidden magnetic order, Eq. (3) in the paper. Heisenberg exchange coupling constants are set by Fig. S1, but without Hund's Rule:  $J_0 = 0$ . Also, the concentration of mobile electrons per site-orbital is set to  $x = 0$  in all mean-field expressions. Black states in Fig. S2a have even parity under orbital exchange  $P_{d,\bar{d}}$ , while red states have odd parity under it. Black spin-1 states therefore represent true spin fluctuations, while red spin-1 states represent hidden spin fluctuations. Notice that the predicted spin-wave spectrum for the hidden Néel state traced by the dashed lines in Fig. S2a successfully describes the dispersion of the exact spin-1 states at low energy<sup>1</sup>. Notice also the tower in Fig. S2a beginning with the spin-0 groundstate at zero 2D momentum, the spin-1 first-excited state at 2D momentum  $(\pi/a)(\hat{x} + \hat{y})$ , the spin-2 second-excited state back at zero 2D momentum, and the spin-3 excited state back at 2D momentum  $(\pi/a)(\hat{x} + \hat{y})$ . This tower of spin- $n$  states clearly coincides with multiply-occupied states of the hidden order spinwave, which is occupied  $n$  times.

Figure S3 shows the exact low-energy spectrum of one electron more than half filling governed by the two-orbital  $t$ - $J$  model, Eq. (1) in the paper, in the absence of Hund's Rule. Heisenberg exchange coupling constants coincide with those in Figs. S1 and S2, while hopping matrix elements are set to  $t_1^\parallel = 2 J_1^\parallel$ ,  $t_1^\perp(\hat{x}) = +5 J_1^\parallel$  and  $t_1^\perp(\hat{y}) = -5 J_1^\parallel$ . Red states are even under orbital exchange  $P_{d,\bar{d}}$ , while blue states are odd under it. The solid blue line depicts the  $d_{yz}$  half metal band predicted by Schwinger-boson-slave-fermion mean field theory at the limit towards half filling,  $x \rightarrow 0$ , but with ideal electron hopping,  $t_1^\parallel = 0$ . The dashed lines trace the dispersion of emergent hole excitations predicted by Eq. (5) and Fig. 1b of the paper. They successfully describe the dispersion of the exact spin-1/2 groundstates per orbital quantum number in the absence of Hund's Rule. Notice, however, the first-excited states per momentum that carry spin 3/2 in Fig. S3. The pairs of spin-1/2 and spin-3/2 states that they make up per momentum can be understood as the result of the addition of angular momentum between a spin-1/2 electron at cSDW wavenumbers and a spin-1 spinwave in the half metal[S4]. In particular, the spin-3/2 state at momentum  $(\pi/a)\hat{x}$  with  $d_{yz}$ -orbital symmetry shown in Fig. S3 can be understood as a spin-1/2 electron in orbital  $d_{xz}$  at momentum  $(\pi/a)\hat{y}$  combined with a hidden-order (odd-parity) spinwave that carries

---

<sup>1</sup> The spectral weight of true ("black") spinwaves at zero 2D momentum is identically zero [cf. Eq. (3) and Fig. 1a in the paper], hence the absence of spin-1 states there in Figs. S2a and S2b.

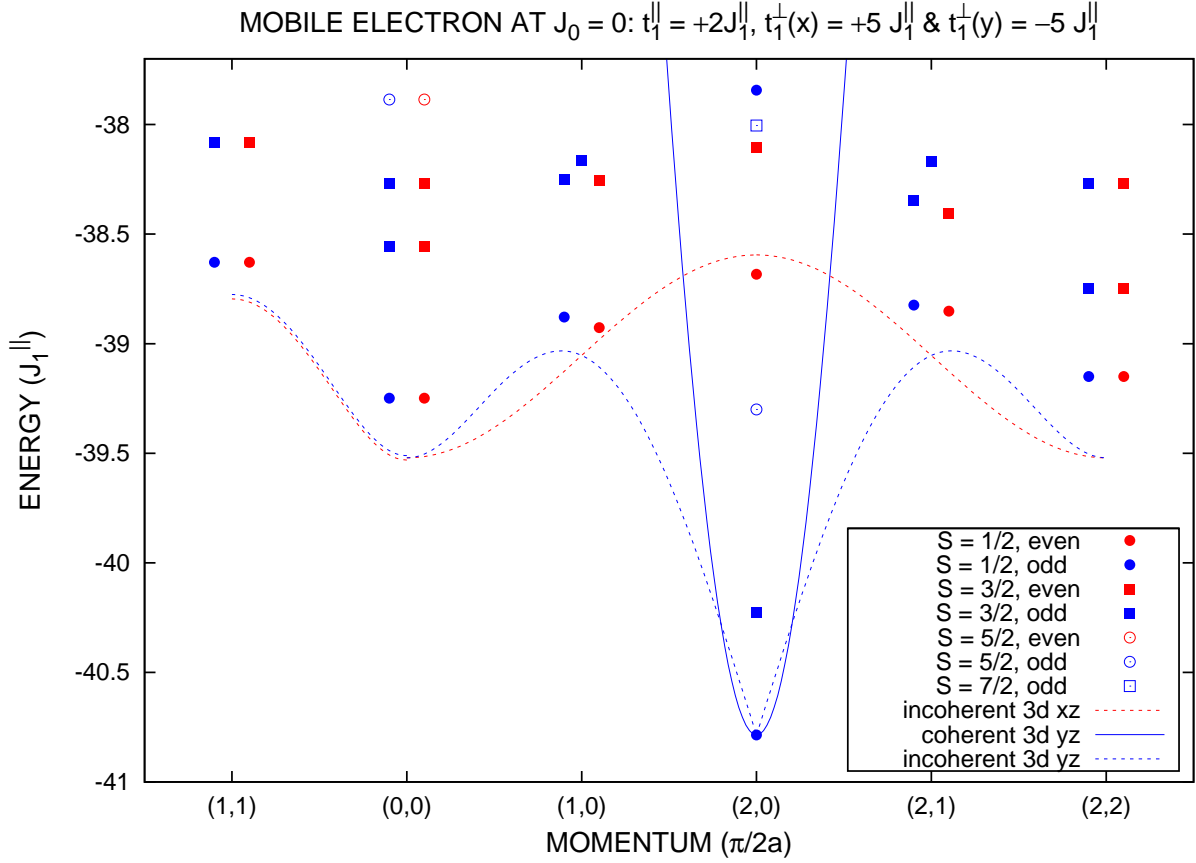


FIG. S3: The exact spectrum of one electron more than half filling for the two-orbital  $t$ - $J$  model over a  $4 \times 4$  periodic lattice in the absence of Hund's Rule. Heisenberg exchange coupling constants coincide with those in Fig. S1. Red and blue dashed lines trace the dispersion of emergent hole excitations in  $d_{xz}$  and  $d_{yz}$  orbitals, respectively, at ideal electron hopping,  $t_1^{\parallel} = 0$ , as predicted by Eq. (5) in the paper.

momentum  $(\pi/a)(\hat{x} + \hat{y})$ . In turn, the second-excited spin-5/2 state at this momentum, which has the same  $d_{yz}$ -orbital symmetry, can be understood as the combination of the spin-1/2 groundstate with *two* hidden-order spin-waves. This tower of states resembles the previous one identified at half filling in Fig. S2a.

Last, Fig. S2b compares the exact spectrum of two electrons more than half-filling in the absence of Hund's Rule with the spin-excitation spectrum predicted by Schwinger-boson-slave-fermion mean field theory at ideal electron hopping  $t_1^{\parallel} = 0$ . Notice that the tower of  $n = 0, 1, 2$  and 3-occupied hidden-order spinwave states persists<sup>1</sup>. Comparison with Fig. S2a indicates that a gap separates out the tower of lowest-energy states in the case of two mobile electrons.

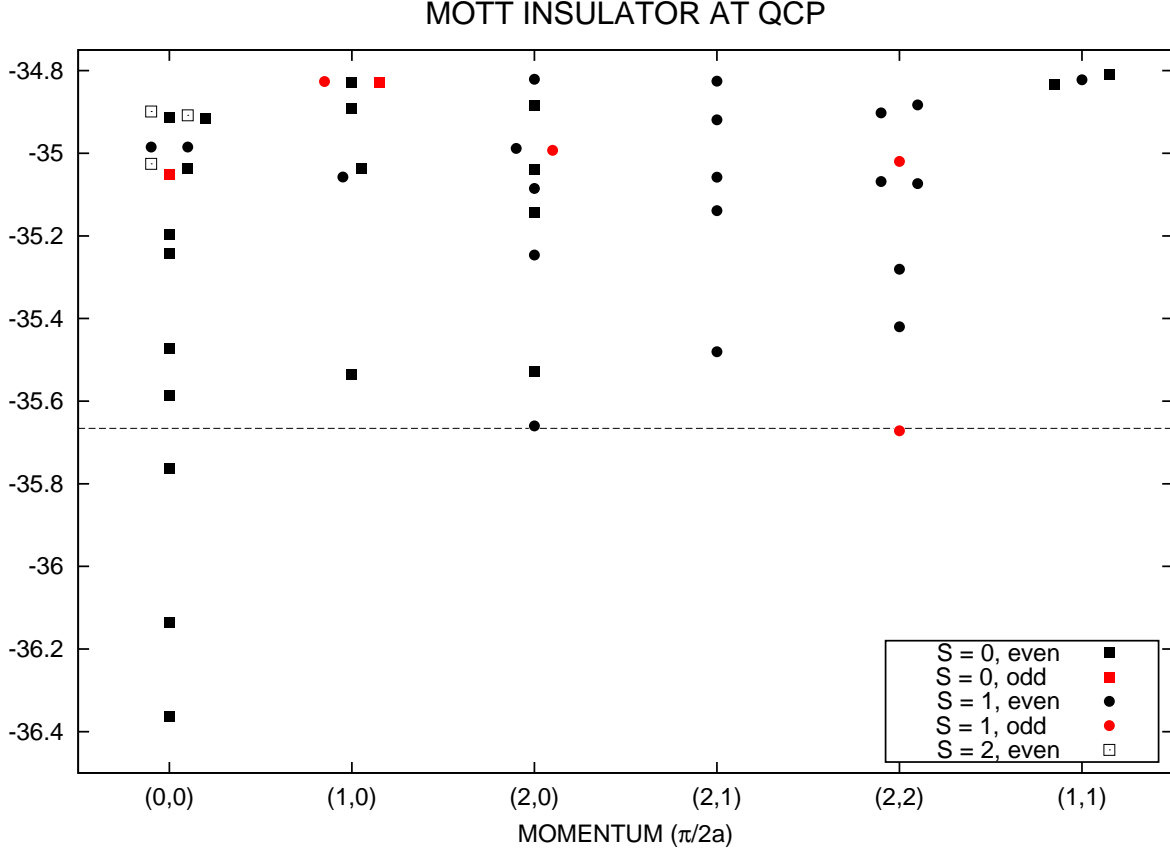


FIG. S4: Heisenberg exchange coupling constants coincide with Fig. S1, but the Hund coupling is tuned to the critical value  $-J_0 = 1.35 J_1^{\parallel}$ .

We therefore conclude that Schwinger-boson-slave-fermion mean field theory is a valid approximation for the two-orbital  $t$ - $J$  model in the case of the hidden half metal state depicted by the insets to Fig. 1 of the paper. (Cf. refs. [S3] and [S4].) In particular, in the absence of Hund's Rule, Fig. S2 demonstrates that it works well for spin-1 states at both half filling and in the case of two mobile electrons. Again, in the absence of Hund's Rule, Fig. S3 demonstrates that Schwinger-boson-slave-fermion mean field theory also works well in the case of one mobile electron for spin-1/2 states.

*QCP.* Figure S4 shows the exact spectrum of the same two-orbital Heisenberg model that corresponds to Fig. S2a, but at the putative quantum-critical point. Here, the Hund coupling is tuned to the critical value  $-J_0 = 1.35 J_1^{\parallel}$  at which the lowest energy spin-1 states at cSDW wavenumbers  $(\pi/a)\hat{x}$  and  $(\pi/a)\hat{y}$  become degenerate with the lowest-energy spin-1 state at Néel wavenumber  $(\pi/a)(\hat{x} + \hat{y})$ . The former states are true spin fluctuations, with even parity under  $P_{d,\vec{d}}$ , while the latter state is a hidden spin fluctuation, with odd parity

under  $P_{d,\bar{d}}$ .

---

- [S1] D.P. Arovas and A. Auerbach, Phys. Rev. B **38**, 316 (1988).
- [S2] A. Auerbach and B. E. Larson, Phys. Rev. B **43**, 7800 (1991).
- [S3] J.P. Rodriguez, M.A.N. Araujo, P.D. Sacramento, Phys. Rev. B **84**, 224504 (2011).
- [S4] J.P. Rodriguez, M.A.N. Araujo, P.D. Sacramento, Eur. Phys. J. B **87**, 163 (2014).
- [S5] A. Auerbach and D.P. Arovas, Phys. Rev. Lett. **61**, 617 (1988).
- [S6] J.P. Rodriguez, Phys. Rev. B **82**, 014505 (2010).
- [S7] J.P. Rodriguez and E.H. Rezayi, Phys. Rev. Lett. **103**, 097204 (2009).